Proceedings of the International Conference on Civil, Structural and Transportation Engineering
Ottawa, Ontario, Canada, May 4 – 5, 2015
Paper No. 267

Adhesive Stresses in Wide Flange Steel Beams Bonded To GFRP Plate under Twist

Phe Van Pham and Magdi Mohareb
A120A, Cononel By building, Ottawa University, Ottawa, ON, Canada
ppham040@uottwa.ca; MagdiEmile.Mohareb@uottawa.ca

***Abstract*-** The present study investigates the three dimensional stress state in adhesive layers bonding wide steel flange beams reinforced with GFRP plate and subjected to twisting moments. A 3D finite element analysis is conducted and contour plots are extracted for the stress fields within the adhesive layer. The most predominant stress fields and locations of peak stresses are identified for typical beam geometry. A parametric study is then performed to investigate the effect of shear modulus of adhesive layer, adhesive layer thickness, and GFRP plate thickness on the resulting maximum von Mises stress within adhesive layer and the resulting twisting deformation. The study identifies practical measures to be taken to reduce stresses within the adhesive layer while ensuring effective composite action for steel members under twist.

1. Literature Review

Fiber reinforced Polymer (FRP) plates are commonly used to retrofit concrete members. Relatively recently, they have been considered as viable retrofitting options for steel members. Zhao and Zhang (2007) identified the types of failure within such composite systems. These are due to: (1) debonding at interfaces, (2) rupture of FRP material, (3) failure of the adhesive material, (4) FRP delamination, and (5) yielding of the steel beam.

Experimental research related to steel beams reinforced with GFRP plates include the studies of Miller et al (2001), El Damatty and Abushagur (2003), Xia and Teng (2005), Schnerch (2005), Zhao and Zhang (2007), and Peiris (2011). Analytical models were also developed in the studies of El Damatty and Abushagur (2003), and Linghoff et al. (2010a, b). Siddique and El Damatty (2013) developed a finite element model for analyzing wide flange steel beams bonded with GFRP plates. Their model captured four failure modes. These are (i) buckling of the system, (ii) shear failure of the adhesive, (iii) peeling failure of the adhesive, and (iv) GFRP failure.

A common feature among the above models is their focus on longitudinal-transverse response of steel beams reinforced with FRP systems. More recently, Pham and Mohareb (2014 a, b) developed a theory and finite element models for longitudinal-transverse response as well as lateral-torsional response. FRP materials include Carbon fiber reinforced Polymers (CFRP) which are typically strong and stiff in tension but with negligible stiffness in compression given their small thicknesses of the order of a few millimetres. In contrast, Glass fiber reinforce polymers (GFRP) are less stiff but come into larger thicknesses (e.g., 10-19mm), and thus are beneficial in tension and compression. Other differences can be founded in Pham and Mohareb (2014 a, b).

2. Motivation and Scope

As most studies have focused on the longitudinal-transverse response of composite systems, the present study aims at developing insight on the predominantly torsional behaviour of steel beams bonded to GFRP plate through an adhesive layer. Since failures of such composite systems can be triggered by adhesive failures, emphasis is placed on stress distributions and magnitudes within the adhesive layer through a parametric study based on a 3D finite element model under Abaqus. Towards this goal, a reference case based on realistic geometric and material parameters is investigated in detail to identify the

important stress fields and distributions. Deviations from the reference case are then examined to develop a systematic parametric study aimed at investigating the effects of adhesive shear modulus, adhesive thickness, and GFRP thickness on the stresses induced into the adhesive layer and the induced twisting response.

3. Reference Case

A 5m span cantilever beam fixed at end $z = 0$ and free at end $z = 5000mm$ consists of a W410x85 steel beam (flange width $b_b = 181mm$, flange thickness $t_f = 18.2mm$, depth $d = 417mm$ and web thickness $t_w = 10.9mm$) is reinforced by a GFRP plate over the whole span (Fig.1). The GFRP plate has a thickness $t_P = 19mm$ and a width $b_p = 181mm$. Modulus of elasticity of steel is $E_s = 200GPa$ while that of GFRP is $E_P = 42GPa$. The shear modulus of the adhesive material is $G_a = 0.4GPa$ its thickness is $t_a = 2mm$.The member tip is subject to tangential tractions in opposite direction to induce a twisting moment $T = 3.27kNm$ about the wide flange centroid. The magnitude of the twisting moment was selected so that the maximum stresses within steel beam and FRP plate stay within the common yielding and rupture strengths of both materials.

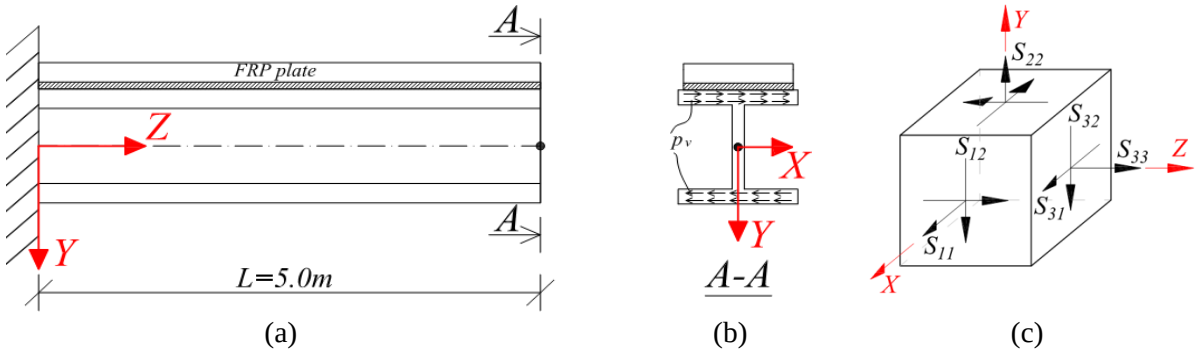

(a) (b) (c)

Fig. 1. Cantilever beam reinforced with GFRP plate (a) Elevation, (b) Cross-sectional view at tip with tractions inducing twist and (c) Stress components of an element.

4. Details of the Finite Element Model

The 3D FEA simulation is conducted using the 8-node brick element C3D8R from the ABAQUS library. The element has 24 degrees of freedom (with three translations at each of the eight nodes) and uses reduced integration to avoid volumetric locking. Thus, the element has a single integration point located at the element centroid. All three displacement components were restrained at all nodes of the fixed end.

A mesh study (Pham and Mohareb 2014 a, b) indicated that convergence is achieved when using 15 elements along the flange half flange width excluding the web, 10 elements across the flange thickness, 50 elements along the web height, 4 elements across the web thickness, 4 elements across the adhesive thickness, 8 elements across the GFRP thickness, and 2500 elements in the longitudinal direction.

5. Stresses within Adhesive Layer

The "view cut" function in Abaqus CAE is used to obtain the stress contour plans at Steel-Adhesive (SA) and Adhesive-Plate (AP) interfaces (Figure 2). Different length scale factors (i.e., the scale factor in the direction of the lateral direction is taken to be seven times larger than that in the longitudinal direction) for better visualization of the results in the contour plots. Of the six stress contours (Fig. 2a-f) the largest stress magnitudes are observed to be those of S_{23} which shows a peak value of 6.548MPa (Fig. 2e). The magnitude of the stresses S_{11}, S_{22}, S_{33}, and S_{12} are observed to be comparatively negligible. Thus,

the Mises stresses (Figs.2g-h) are observed to almost be entirely due the shear stress S_{23}. Stresses S_{11}, S_{22}, S_{33}, and S_{12} show localization near the free edge (at the top edge of the contour plots) and at the fixed end (at the bottom edge of the contour plots). Figure 3 shows the sectional contour profiles for stresses S_{23} at z=3,454mm. Different length scale factors (i.e., the scale factor in the direction of the transverse direction is taken to be seven times larger than that in the lateral direction) for better visualization of the results. All stress fields except S_{13} are observed to be constant across the adhesive layer depth. Thus, for stress S_{13}, two contour plots are provided (Figs. 2f-i) to show the stress gradient across the thickness. S13 is observed to range from a compressive stress of 0.139 MPa to a tensile stress of 0.0449 MPa. Both bounds are negligible compared to the stresses S_{23}.

Two contour plots are provided for the von Mises stresses at the SA and AP interfaces (Figs. 2g-h). Figures 2g-h are practically indistinguishable, suggesting that the von Mises stresses are nearly constant across the depth. It is worthwhile to note that the location of peak Mises occurs neither at the free nor the fixed end, but around $0.7L$ from the fixed end at z=3,454mm and is located at the edge (Figs. 2g-h, and Fig. 4). Table 2 provides the six stress components at the location of the peak von Mises stress S_M given by

$$S_M = \sqrt{\frac{1}{2}\left[\left(S_{11}-S_{22}\right)^2+\left(S_{22}-S_{33}\right)^2+\left(S_{11}-S_{33}\right)^2+6\left(S_{12}{}^2+S_{23}^2+S_{31}^2\right)\right]} \qquad (1)$$

Table 2. Stress fields at the location of maximum Mises stress (z=3,454mm)

Stress	S_{11}	S_{22}	S_{33}	S_{12}	S_{13}	S_{23}	S_M
Value (kPa)	0.073	0.18	-66.22	0.188	-57.34	-6,548.21	11,342.5

It is noted that by disregarding $S_{11}, S_{22}, S_{33}, S_{12}$, and S_{13}, and retaining the stress S_{23}, one obtains a Mises stress $S_M = \sqrt{3}S_{23} = \sqrt{3}S_{23} = \sqrt{3}\times 6.55 = 11.3MPa$ which is 99.9% of the Mises stress including all six stress contributions. Thus, for all practical purposes, all but the shear stress S_{23} can be considered negligible.

6. Parametric study

This section aims at investigating the effect of three parameters: a) adhesive shear modulus, adhesive thickness, GFRP plate thickness on the the peak angle of twist as well as the peak stress S_{23} and von Mises stresses within the adhesive layer. Twenty additional parametric runs were conducted by varying one parameter at a time. The matrix of parametric runs is presented in Table 3.

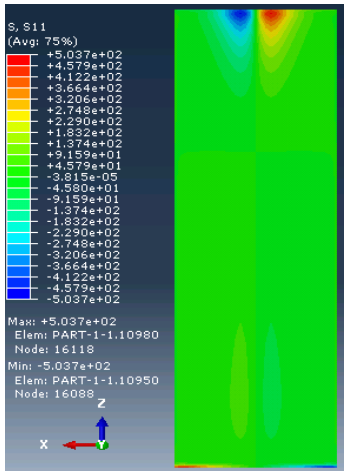

(a) S_{11}

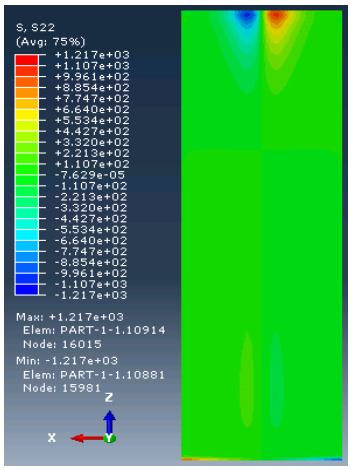

(b) S_{22}

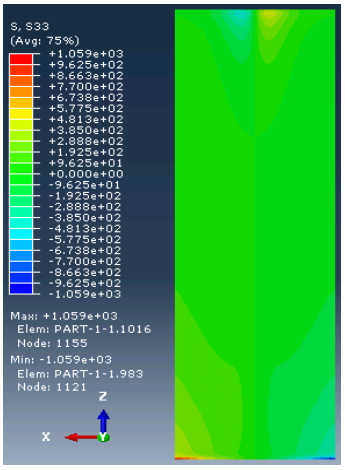

(c) S_{33}

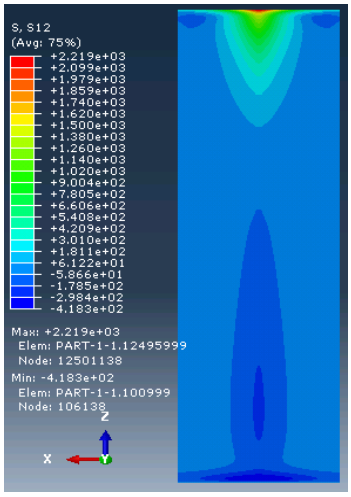

(d) S_{12}

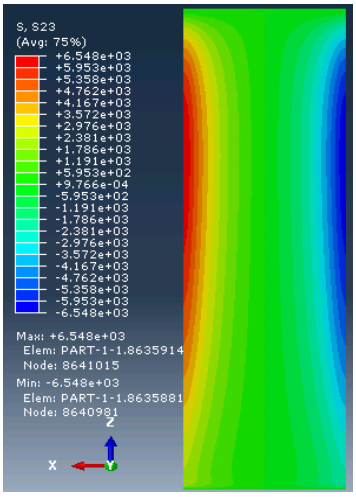

(e) S_{23}

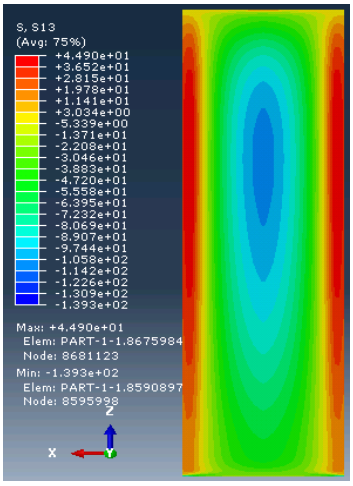

(f) S_{13} - AP interface

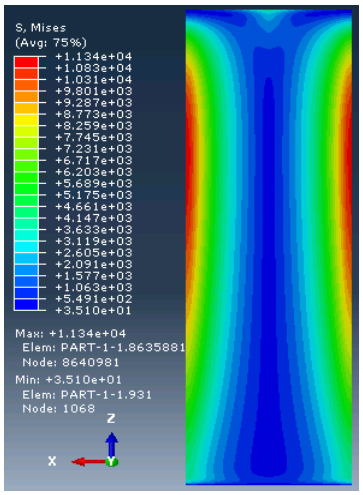

(g) Mises stress-SA interface

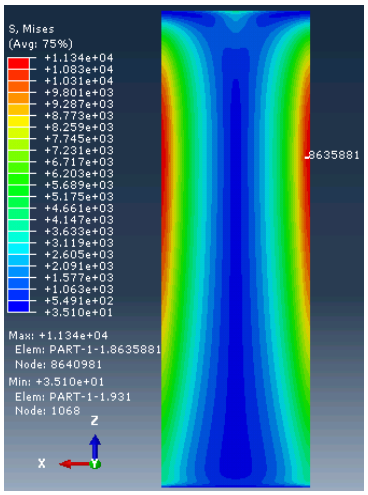

(h) Mises stress -AP interface

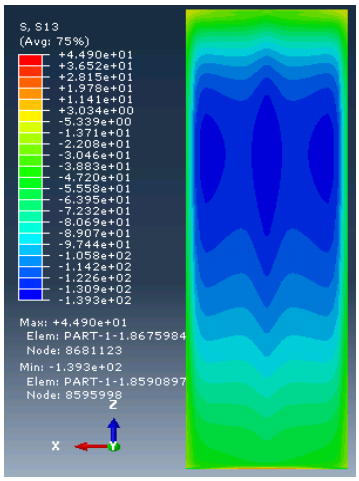

(i) S_{13} - SA interface

Fig. 2. Plan view of the contours of stress fields at the adhesive-steel interface (Length scale factor for X dimension =7).

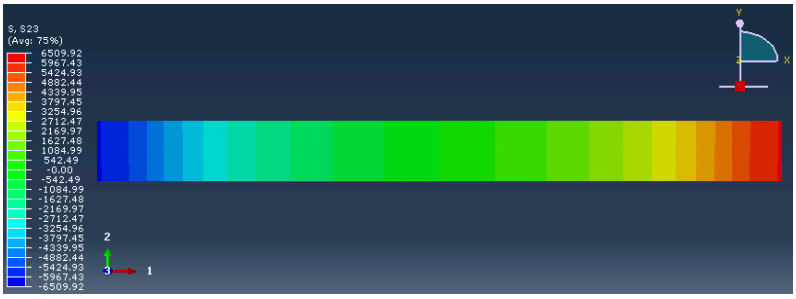

Fig. 3. Cross-section view for stress field S_{23} at z=3,454 mm
(Length scale factor for Y dimension =7)

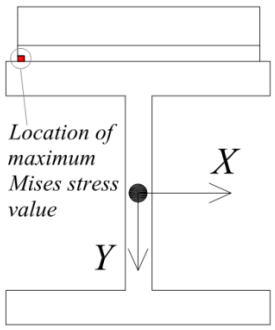

Fig. 4. Cross-section view

Table 3. Parametric study

Case	Adhesive shear modulus G_a (MPa)	Adhesive Thickness t_a (mm)	Ratio G_a / t_a (MPa/mm)	GFRP thickness t_P (mm)	Maximum Stress within the adhesive layer (MPa)				Twisting Angle at the cantilever tip (Rad)
					von Mises	S_{23}	Longitudinal coordinate z (mm)/Interface		
Refer-ence	400	2	200	19	11.34	-6.548	3,454	SA	0.122
1	5.0	2	2.5	19	0.624	-0.360	3,804	AP	0.168
2	50	2	25	19	4.252	-2.455	3,654	SA	0.150
3	100	2	50	19	6.398	-3.694	3,578	SA	0.140
4	400	1	400	19	13.86	-8.003	3,442	SA	0.120
5	400	4	100	19	9.146	-5.280	3,468	SA	0.124
6	400	6	66.7	19	7.996	-4.616	3,472	SA	0.125
7	50	0.5	100	19	8.488	-4.900	3,540	SA	0.134
8	100	1	100	19	8.597	-4.963	3,530	SA	0.133
9	200	2	100	19	8.798	-5.079	3,508	SA	0.130
10	400	4	100	19	9.146	-5.280	3,468	SA	0.124
11	400	2	200	10	9.195	-5.306	3,680	SA	0.154
12	400	2	200	15	10.78	-6.221	3,550	SA	0.136
13	400	2	200	22	11.47	-6.623	3,390	SA	0.113
14	400	2	200	25	11.42	-6.590	3,334	SA	0.105
15	400	2	200	30	11.04	-6.374	3,248	SA	0.092
16	400	2	200	32	10.81	-6.243	3,218	SA	0.088
17	400	2	200	33	10.70	-6.176	3,204	SA	0.086
18	400	2	200	34	10.58	-6.106	3,190	AP	0.084
19	400	2	200	35	10.45	-6.034	3,176	AP	0.082
20	400	2	200	40	9.785	-5.649	3,114	AP	0.073

7. Effect of Shear Modulus

In runs 1 through 3, the shear modulus was varied from its value in the reference case. Figure 5 depicts the peak Mises stress in the adhesive versus the shear modulus of the adhesive. Also, depicted on the same plot is the angle of twist versus the shear modulus in the adhesive. As the shear modulus of adhesive layer increases, the peak value of the von Mises stress is observed to increase. Conversely, an increase in the shear modulus of the adhesive is observed to correspond to a decrease in angle of twist as a result of the stronger interaction provided by the adhesive between the steel beam and the GFRP plate

The location of the peak Mises stress is observed to occur at the AP interface when the shear modulus of adhesive material is small (e.g., Case 1). In contrast, the location of peak Mises stress moves to the SA interface when the shear modulus of the adhesive is small. Also, the peak Mises stress is observed to be farther from the tip when the adhesive shear modulus increases.

8. Effect of Adhesive Thickness

In runs 4 through 6, the thickness was varied from its value in the reference case. Figure 6 depicts the peak Mises stress in the adhesive versus its thickness. Also, depicted on the same plot, is the angle of twist versus the thickness. As the thickness of adhesive layer increases, the peak value of the von Mises stress is observed to decrease. Conversely, the angle of twist increases as the interaction between the steel beam and the GFRP plate becomes smaller. In all cases, the location of the peak Mises stress is observed to take place only at the SA interface (Fig.4) and to gradually move towards to the tip of the cantilever beam when the adhesive thickness increases.

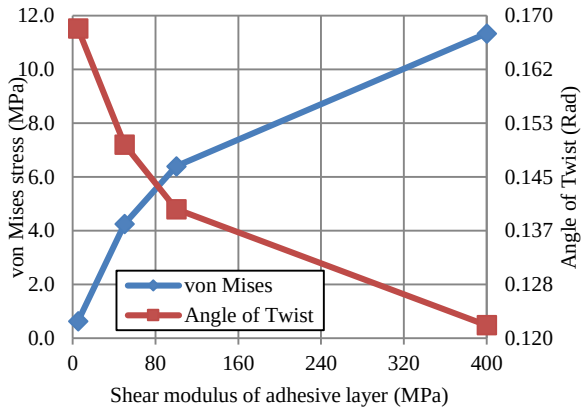

Fig. 5. Relationship between shear modulus of adhesive layer to von Mises stress and angle of twist

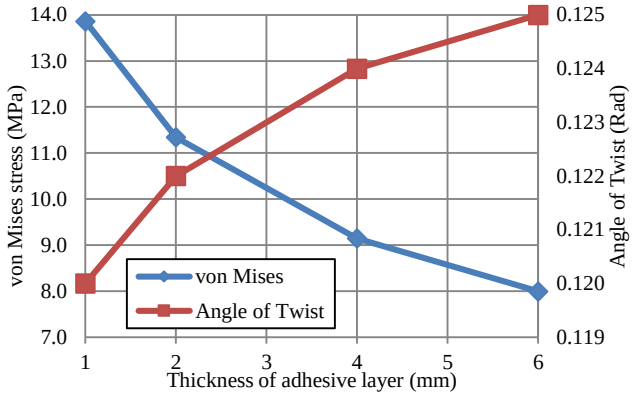

Fig. 6. Relationship between thickness of adhesive layer to von Mises stress and angle of twist

9. Effect of the G_a / t_a Ratio

In the work of Pham and Mohareb (2014 a, b), it was observed the total strain energy within the adhesive layer remains essentially unchanged when the adhesive thickness t_a is small and the ratio G_a / t_a is kept constant, i.e., the degree of interaction between steel beam and GFPR plate remained essentially unchanged for a given G_a / t_a value. A similar observation is observed in runs 7-9 which give essentially the same twisting response, while run 10 for which $t_a = 4mm$ predicted a small reduction in the angle of twist. It is recalled that in the present literature, thicknesses larger than $t_a = 2mm$ were observed to be uncommon.

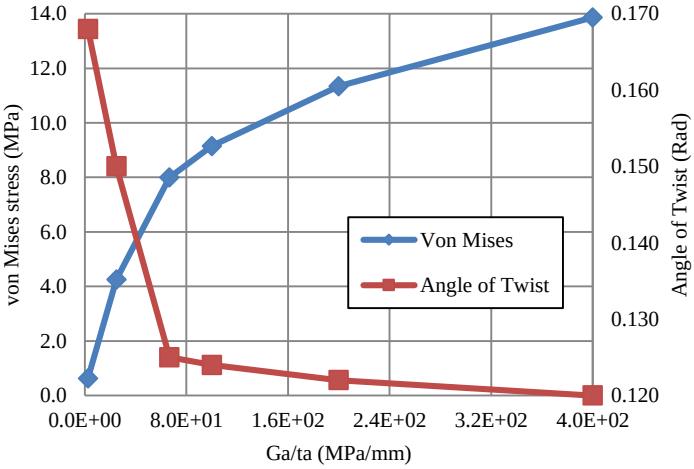

Fig. 7. Relationship between ratio G_a / t_a to von Mises stress and angle of twist

Figure 7 depicts the peak Mises stress in the adhesive versus the ratio G_a / t_a for runs 1 through 5 along with the reference case. Also, depicted on the same plot is the angle of twist versus the ratio. As the

ratio increases, the peak value of the von Mises stress is observed to increase. Conversely, the angle of twist decreases as the interaction between the steel beam and the GFRP plate is increased.

10. Effect of GFRP Plate Thickness

In runs 11 through 20 of Table 3, the GFRP plate thickness was varied from its value in the reference case. The location of the peak von Mises stress is observed to be closer to the fixed end when the GFRP plate thickness increases (Table 3). Across the height, the peak Mises stress is observed to occur either at the SA or AP interface, depending on the magnitude of the shear stress S_{13} across the adhesive depth. Figure 8 depicts the peak Mises stress in the adhesive versus the thickness of the GFRP plate. Also, depicted on the same plot is the angle of twist versus the thickness. As the thickness of the GFRP plate increases, the angle of twist is observed to gradually decrease. However, the peak von Mises stress is observed to increase and reaches a peak value at a plate thickness of 22mm (run 13), and then starts to decrease. A thicker GFRP plate is observed to be associated with two benefits: a) a decrease in the angle of twist of the beam and b) a decrease in the von-Mises stress in the adhesive. A thicker GFRP plate is observed to be associated with higher Mises stresses in the top of the web (Fig.9).

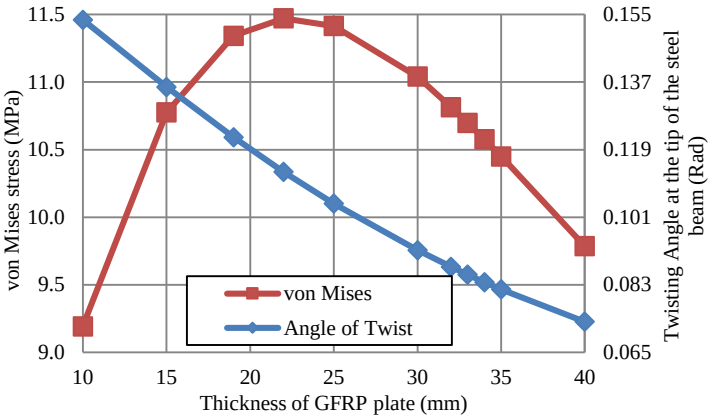

Fig. 8. Relationship between thickness of adhesive layer to Von Mises stress and angle of twist

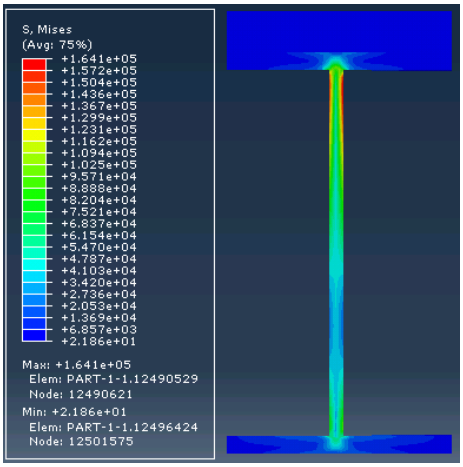

Fig. 9. Cross-section contour

11. Conclusions

Based on the present study, the following conclusions can be drawn:

1. The most predominant stress field within adhesive layer is the shear stress S_{23}. It is found to be responsible for 99.9% of the von Mises stress.
2. The five stress fields $S_{11}, S_{22}, S_{33}, S_{12}, S_{23}$ are observed to be nearly constant across the adhesive thickness. In contrast the shear stress S_{13} and von Mises stress is to have a gradient across the thickness.
3. The peak Mises stresses are observed to occur at the outer edges of steel-adhesive or adhesive-plate interfaces.
4. An increase in the shear modulus of adhesive corresponds to an increase in the von Mises stress within adhesive layer and a decrease in the angle of twist at the tip, and the closer the point of peak von Mises stress becomes to the fixed end.
5. When the thickness of adhesive layer is small enough (<2mm), the angle of twist of the system is observed to remain almost unchanged when the ratio shear modulus/thickness of adhesive layer is constant.
6. An investigation of the effect of GFRP thickness on the response has shown that an average thickness (19-30mm) of the plate should be used for real application. Thinner GFRP plates are

less effective in reducing the angle of twist and thicker ones will experience high localized stresses in the web.

References

El Damatty, A.A. and Abushagur, M. (2003), Testing and modeling of shear and peel behavior for bonded steel/FRP connections, Thin-Walled Structures, 41(11), 987-1003.

El Damatty, A., Abushagur, M. and Youssef, M. A. (2003), Experimental and analytical investigation of steel beams rehabilitated using GFRP sheets, Journal of Steel & Composite Structures 3(6), 421-438.

Linghoff, D. and Al-Emrani, M. (2010), Performance of steel beams strengthened with CFRP laminate – Part 2: Laboratory tests, Composites Part B, 41(7), 516-522.

Linghoff, D., Al-Emrani and Kliger, M. R. (2010), Performance of steel beams strengthened with CFRP laminate – Part 1: Laboratory tests, Composites Part B, 41(7), 509-515.

Miller, C.T., Chajes J.M. and Hastings N.J. (2001), Strengthening of a steel bridge girder using CFRP plates, Journal of Bridge Engineering 6(6), 514-522.

Peiris, N.A. (2011), Steel Beams Strengthened with ultra High Modulus CFRP Laminates, Doctoral Thesis, College of Engineering, University Kentucky.

Pham, P.V., (2013), Stress-Deformation Theories for the Analysis of Steel Beams Reinforced with GFRP Plates, Master of Science Thesis, Department of Civil Engineering, University of Ottawa, Ottawa, ON, Canada.

Pham, P.V. and M. Mohareb (2014), A shear deformable theory for the analysis of steel beams reinforced with GFRP plates, Thin Walled Structure, 85, 165-182.

Pham, P.V. and M. Mohareb (2014), Finite-Element Formulations for the Spatial Static Response of Steel Beams Bonded to a GFRP Plate, Journal of Engineering Mechanics, 10.1061/(ASCE)EM.1943-7889.0000862, 04014143.

Schnerch, D., Dawood, M., Rizkalla, S., Sumner, E. and Stanford, K. (2005), Bond behavior of CFRP strengthened steel structures, Advances in Structural Engineering, 9(6), 805-817.

Siddique, M.A.A. and El Damatty, A.A. (2013), Improvement of local buckling behaviour of steel beams through bonding GFRP plates, Composite Structures, 96(6), 44-56.

Xia, S.H. and Teng, J.G., Behaviour of FRP-To-Steel Bonded Joints, Proceedings of International Symposium on Bond Behaviour of FRP in Structures, 2005, 411-418.

Zhao, X.-L. and Zhang, L. (2007), State-of-the-art review on FRP strengthened steel structures, Engineering Structures, 29(8), 1808-1823.